Preprint of book chapter 8 of "Nonlinear Optics and Application," ed. H. A. Abdeldayem and D. O. Frazier, Research Signpost, pp. 207-232, ISBN: 978-81-7736-073-8 (2007).
http://www.ressign.com/UserBookDetail.aspx?bkid=622&catid=149

Confined nonlinear II-IV-V_2 waveguide structures for compact chemical and biological sensors

Nikolaus Dietz*[a] and Frank L. Madarasz[b]

[a] Department of Physics & Astronomy, Georgia State University, Atlanta, GA 30303

[b] East West Enterprises, Inc., Huntsville, AL 35816

ABSTRACT

Confined nonlinear device structures based on group II-IV-V_2 chalcopyrite compound semiconductors offer unique advantages over group III-V and IV compounds due to their birefringent nature and lower crystal symmetry. For instance, the birefringent properties are used in three-wave nonlinear parametric processes with very high values of the second-order hyperpolarizabilities. In addition, the recent discovery of room-temperature ferromagnetism in dilute magnetic chalcopyrite semiconductors adds an additional functionality to this material system that makes possible the construction of novel magneto-optical device structures based on confined ferromagnetic layers and nanocomposites, which can be embedded in confined birefringent layers. These nonlinear structures form the key elements of the Solid-State Molecular Sensor and related device structures central to this chapter. Solid-State Molecular Sensor structures are designed to detect and discriminate between numerous and varied molecular species. It does so by sensing phase and amplitude shifts due to the presence of a chemical/biological agent on the collector surface. These shifts are then translated into a characteristic - molecule specific - intensity spectrum as a function of frequency. This information can be more accurately analyzed than the limited information returned by devices based on linear optical responses. In addition, the detection, discrimination and estimation of the concentrations of multiple targeted molecular species critically depend on a highly accurate signal processing methodology, which is capable of de-convolving the various spectra. For this we apply Bayesian inference, an extremely powerful technique that is complementary to our data acquisition. "Solid State Molecular Sensor" structures have a myriad of potential applications that include: recognition of environmental hazards; quick and remote screening of air pollutants; monitoring of surface corrosion/etching processes; bio-medical testing; nonlinear optical modulators; and magneto-optical switches.

* Email: ndietz@gsu.edu

1. INTRODUCTION

The need for a rugged, miniaturized sensor to identify, discriminate, and quantify targeted chemical/biological (CB) agents in real time is crucial and of high priority. The proposed, highly integrated technology Solid State Molecular Sensor (SSMS) and variants, along with SSMS networks fits these critical operational criteria. Several optical detection concepts are being explored utilizing optical fibers and linear waveguided structures. A review of the various techniques has been provided by Boisdé et al.[1] Each have a niche market for a specific application. Most, however, lack the potential for further development due to limitations either in sensitivity, integration, handling, or discrimination capabilities.

The essential criteria for the development of a compact, integrated CB detection system are different from the applications requirements that mandate probing over large distances/volumes. In this case, integration is less important, and the key technological task is the development of high-intensity lasers operating at wavelengths in the mid- (3-5 microns) and far-IR (8-12 microns).[2-6] The limitations imposed by the transparency windows of the earth's atmosphere in such high power applications fortunately do not apply to the highly localized SSMS systems, which generally provides for a wider range of detection. In the development of compact, highly integrated SSMS systems it is necessary to keep in mind that substantial *initial efforts must be made that focus on materials, device design, simulation and validation of performance*.

The SSMS concept[7-10] is based on birefringent, confined nonlinear chalcopyrite (CP) heterostructures. It differs significantly from conventional passive waveguide sensors where the evanescent wave (phase and amplitude) is analyzed either interferometrically (phase shift) or by integral means (absorption loss). It uses a nonlinear, birefringent medium to translate phase and amplitude changes, encountered in the evanescent wave, into frequency shifts associated with an optical parametric oscillator (OPO) process.

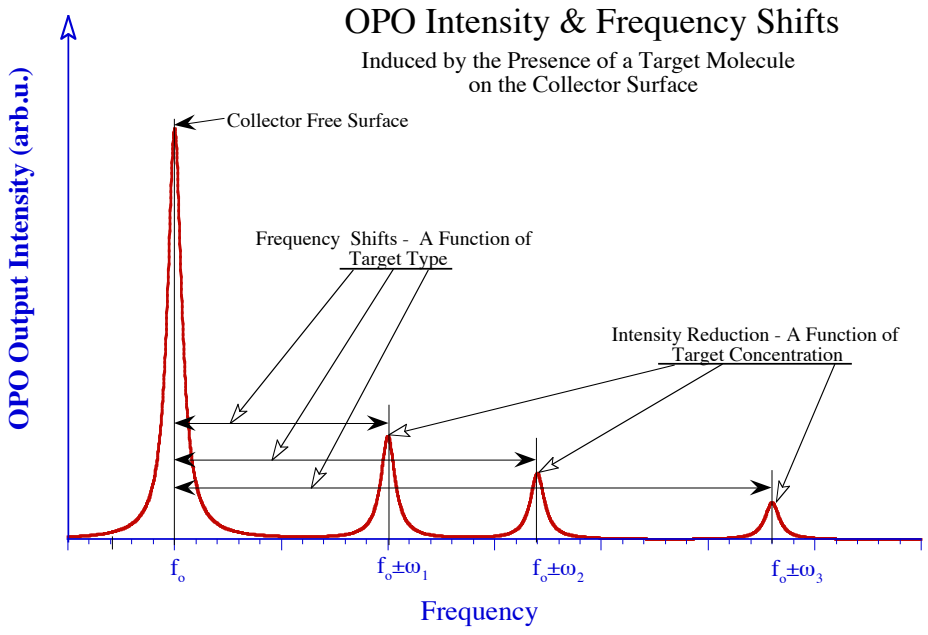

Fig. 1. OPO sidebands induced by the presence of a target molecule(s) on the collector surface.

Figure 1 illustrates the physical principles of detection and discrimination employed by the SSMS. Assuming that the phase matching condition is established for a given pump laser

wavelength, an evanescence wave probing an impurity free collector surface in an optical parametric oscillation (OPO) process will generate an output wave with base frequency, $f_{o,}$ and corresponding intensity peak. The presence of a target CB agent produces a phase shift resulting in a series of side bands: frequency shifted and intensity reduced. These side bands may be viewed as a unique, target specific, frequency spectrum whose peak intensities are a function of the collector surface concentration.

2. SOLID-STATE MOLECULAR SENSOR (SSMS): COMPONENTS

Figure 2 schematically depicts an integrated SSMS structure that consists of several basic elements labeled in the figure: (1) pump laser; (2) optical confined CP heterostructure for the generation of coherent infrared (IR) light with an integrated sensing area where the probe beam interacts with the collector surface; (3) detection unit(s); and, (4) an analysis/discrimination unit, which incorporates integrated circuitry for logic feedback. All of these components can be monolithically integrated onto one substrate or organized into a hybrid structure, which combine nonlinear optical (NLO) and electronic structures, using micro-bonding techniques. Alternatively, they may be linked to each other by waveguides or optical fibers.

The essential components of a SSMS device structure are the birefringent CP layers. These layers are essentially optically confined. However, they are engineered to optically "leak" between adjacent layers, including the collector surface, for nonlinear mixing and sensing purposes. One possible implementation of a birefringent CP based sensor structure is schematically illustrated in Figure 3. In this structure, refractive index graded layers are used to guide waves of the different wavelengths within the same layer. The nonlinear generated Signal and Idler waves propagate in the same spatial region as the pump wave.

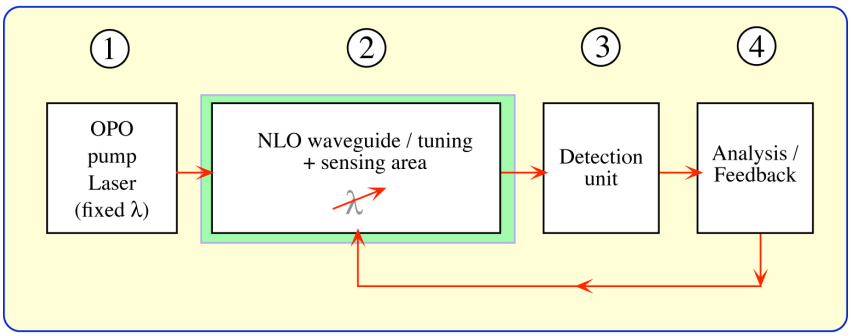

Fig. 2. Schematic of an integrated SSMS system.

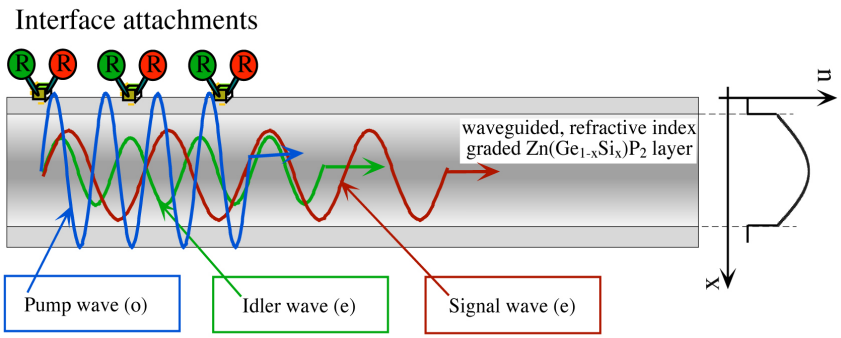

Fig. 3. Wave propagation in a refractive index graded, optically confined CP layer. The side band frequencies and intensities of the generated Idler and Signal waves are directly affected by the interaction of the pump wave with collector surface (see Fig. 1).

The base frequencies of both generated waves are given by the phase matching conditions that correspond to the direction of the optical axis of the crystal relative to the direction of wave propagation (see section 4). The interaction of the pump wave with the collector surface induces phase and amplitude shifts that directly affect the generated idler and signal waves, which is illustrated in Fig. 1

There are several other possible SSMS device structures that have been outlined in an earlier publication[8]. For instance, utilizing spatially coupled waveguides, formed by multiple heterostructures, enables the spatial separation of pump wave and nonlinear generated signal and idler waves, which can improve sensitivity and the discrimination capability. Such an optical parametric generator configuration is schematically shown in Fig. 4. The top waveguide is a single-mode, nonlinear, open resonator. Its indices and layer thicknesses are chosen such that waves will propagate in the lowest modes. With the optical axis lying in the plane of the waveguide, phase matching is dependent on the angular orientation between it and the propagation vector of the wave. In addition, it is dependent on the orientation of the polarization of the pump wave with respect to the axis of the guide. Phase matching and the strength of the interactions depend explicitly on the thickness and geometry of the guide. Moreover, this structure has the added flexibility that phase matched coupling can occur between the various modes of the guide, which is absent in bulk materials. The configurations illustrated in Fig. 4 add flexibility to the design, manufacturing and operation of the integrated sensors, parametric light sources (fixed-frequency and tunable) and frequency-agile laser light sources. The two waveguides for the propagation of the signal and idler waves can be formed a linear waveguides carrying the waves to the analysis/detection area(s).

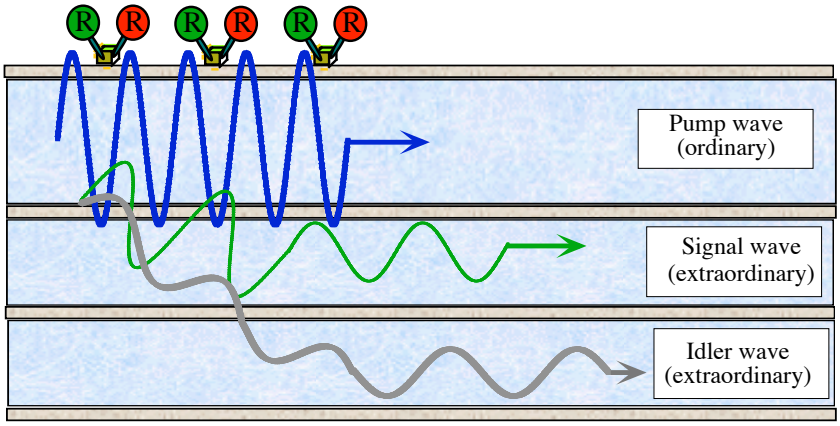

Fig. 4. Spatial separation of generated signal and idler waves upon generation. As in Fig. 3, the interaction of the pump wave with the collector surface leads to side band frequencies and intensities in the generated Idler and Signal waves.

The principal advantage of having the generated signal and idler waves separated from the area of generation manifests itself in a significant decrease of the background scattering and noise. It also enables the differential analysis of waves generated at the collector surface versus a reference area with well-defined characteristics. This is especially useful when using these devices as integrated sensors in the detection and discrimination of specific molecular targets adsorbed (attached) at the upper cladding in Fig. 4, denoted as collector surface. The collector surface can be chemically sensitized to allow absorption of specific targeted molecules.

The schematic in Fig. 5a illustrates how the collector surface area may be minimized by the use

of 2-dimensional (2-dim) heterostructures. Such a structure increases the strength of NLO interactions and reduces problems associated with beam drift, i.e., walk-off, from the direction of propagation. As shown in the next section, such 2-dim CP structures can for instance be formed in GaP/$ZnGeP_2$/GaP multiple heterostructures, which represents a nearly lattice matched materials combination. Since applications in the IR wavelength regime require refractive index modulations on a micrometer scale, the fabrication of 2-dim CP structures is easily accessible by conventional photolithography and heteroepitaxial growth methods. The SSMS device configuration shown on Fig. 5a uses multiple layered nonlinear and linear optically confined layers for wave separation as shown in Fig. 4. The substrate and cladding layers between the waveguides are not shown for simplicity. The collector surface and the NLO active area are in this case are identical, meaning that a modification of the collector surface directly affects the NLO process. As was discussed in section 1, molecules that are attached to the collector surface alter the probe wave in two essential ways. Their presence effects a local change in the dielectric function of the collectors. In turn, the probe wave experiences a phase shift and an absorption induced reduction in its complex amplitude. Both effects will couple nonlinearly back to the underlying CP layer and alter the OPO process as illustrated in Fig. 1. The OPO frequency shift and the generated side bands, though small, can be measured by an optical beating technique based on coherency of the signal wave. After the wave separation, each wave can be analyzed using integrated 2-dim super prism structures as diffraction gratings and frequency filters, followed by an adjacent detector array.

A slightly different SSMS configuration is illustrated in Fig. 5b, where 1-dim or 2-dim CP structures are used for frequency agile IR laser light generation. The frequency agile laser light can be tuned in a wide spectral range (e.g. 2mm - 10 mm for confined $ZnGeP_2$ structures) and is used to probe resonant any CB agent of interest in a micro fluid/gas channel. The fluorescence excited by the laser light is frequency dispersed analyzed as in the first configuration shown in Fig. 5a.

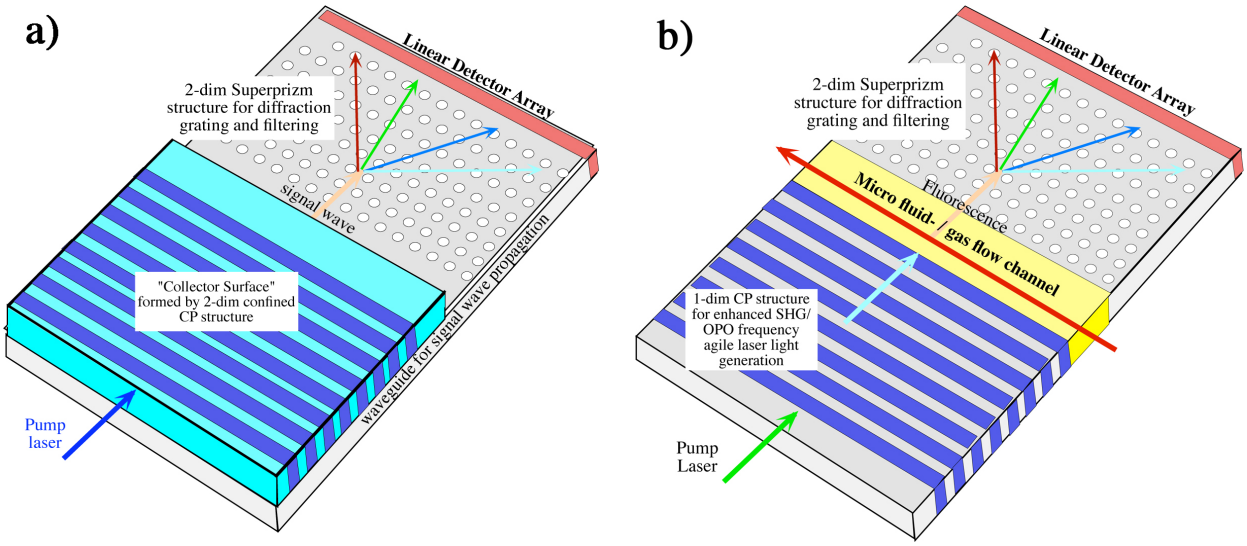

Fig. 5. a) Schematic of a SSMS device configuration using a 2-dim CP structures for high sensitive surface attachments characterization (substrate and cladding layers are not shown for simplicity). **b)** SSMS device configuration where 1-dim or 2-dim CP structures are used as frequency agile IR laser light generators in order to characterize

CB agents in a micro fluid/gas channel (the frequency dispersed fluorescence is analyzed).

So far, the potential of ternary II-IV-V_2 bulk CP compound semiconductor materials has been mostly explored in the context of their potential for nonlinear optical applications.[11-14] Although CP semiconductors have electric, magnetic and optical properties comparable or superior to their group IV, III-V or II-VI counterparts, for many applications CP semiconductors have advantages due to their comparatively lower crystal symmetry. Being optically birefringent and pleochroic, their optical and electro-optical properties are highly orientation dependent, thereby making them more sensitive to their environment. In principle, it will enable new capabilities in thin-film coupled-waveguide optoelectronic devices, where the possibility of controlling layer composition, thickness, and spacing is expected to lead to new levels of performance in linear and nonlinear devices. Moreover, the demonstrated ferromagnetic properties in several CP materials and their compatibility with III-V compound semiconductors opens new opportunities in exploring magnetically controlled NLO heterostructures and nanocomposites[8]. Such a structure can be embedded in optically confined cladding layers to form a nonlinear waveguided magnetic photonic crystal (MPC) structure, analogously to photonic crystals.[15] In addition to photonic band gap engineering, MPC structures will enable the exploration of linear and nonlinear optical device structures based on magneto-optical interactions in single quantum dots and coupled quantum dot arrays.
The successful fabrication of such device structures will open new fields of applications, e.g. magneto-optical modulators, magneto-optic read/write storage devices, magnetic spin-controlled frequency-agile laser sources, or spin-electronic devices.

3. CONFINED NONLINEAR II-IV-V_2 WAVEGUIDE STRUCTURES

3.1. II-IV-V_2 COMPOUND SEMICONDUCTORS

Ternary group II-IV-V_2 CP compound semiconductor materials have been investigated extensively during the last few decades mainly for their unique birefringent properties[11,12,14]. The recent discovery of room-temperature ferromagnetism in Mn-doped group II-Ge-V_2 CP compounds[16-20] demonstrates the emerging potential of II-IV-V_2 CP compounds as truly multifunctional materials. Although CP semiconductors have electrical and optical properties comparable or superior to their group IV, III-V or II-VI counterparts, for many applications they have decided advantages due to their lower crystal symmetry. Being optically birefringent, pleochroic and ferromagnetic, their magneto-optical and electro-optical properties are highly orientation dependent, thereby making them highly sensitive to their environment. Utilizing these properties will enable the fabrication of unique devices, especially the fabrication of one-dimensional (1-dim) or two-dimensional (2-dim) electrical and/or optical confined material structures. That is, confined heterostructures, where the possibility of controlling layer compositions, thicknesses, and spacings are expected to lead to unique levels of performance in linear and nonlinear devices. The exploration of embedded 3-dim confined group II-IV-V_2 CP compounds, e.g. ferromagnetic and birefringent quantum dots and nanocomposites may even further extend the unique properties of group II-IV-V_2 CP compounds.

Depicted in Fig. 6, group II-IV-V_2 CP compound semiconductors, space group $I\bar{4}2d$, are the isoelectric analogs of the zincblende gallium phosphide (GaP), space group $F\bar{4}3m$, whereby, the

average number of bonding electrons per atom remains unchanged. For this reason they are known as pseudo III-V compounds. The ordered arrangement of the two cations, tetrahedral coordinated to the anion atoms, in CP unit cell leads to twice the c-axis height of the analogous zincblende cell. However, the differences in the two cationic species surrounding the anion and the manner of ordered substitution accounts for a peculiar distortion in the c-axis. For example, $ZnGeP_2$ and $CdGeAs_2$ have slight compressions along the c-axis, that is, c/a=1.966[21] and c/a=1.888[21], respectively. These compressions have a pronounced effect on their observed nonlinear electrical and optical properties.

The highest nonlinear coefficients in the class of II-IV-V_2 semiconductors reported for the compound systems $(Zn_{1-x}Cd_x)GeAs_2$, $Zn(Ge_{1-x}Si_x)As_2$ and $Zn(Ge_{1-x}Si_x)P_2$. All these CP semiconductors have a positive birefringence. The associated second-order nonlinear susceptibility, $\chi^{(2)}$, increases correspondingly with the substitution of As for P, Ge for Si, and Cd for Zn [13]. $CdGeAs_2$ is reported to have the highest nonlinear optical coefficient in the class of phase-matchable compounds[22]. Note that even the compound $ZnGeP_2$ has a nonlinear optical coefficient approximately 160 times greater than KDP, making it one of the most efficient nonlinear crystal in the wavelength range 0.7 – 12 mm.

Significant progress has been made during the last decades in optimizing the growth of some of the CP bulk compounds (in particular, $CdGeAs_2$[23] and $ZnGeP_2$). However, more extensive research will be required to understand, optimize and control the defect chemistry as well as the surface and surface-interface properties of thin film CP heterostructures and embedded nanocomposites. As demonstrated, thin film growth techniques offer a unique pathway to form and stabilize group III-V and II-VI compound semiconductors that cannot be achieved with bulk crystal growth techniques.

3.2 CONFINED MULTIFUNCTIONAL GROUP II-IV-V_2 CP HETEROSTRUCTURES

The growth and study of confined birefringent and ferromagnetic CP hetero- and nanostructures as needed for advanced multifunctional devices, is of crucial importance. Not only does this include growth techniques and materials optimization, but also the design and prediction of the optical interactions in confined birefringent heterostructures and optically coupled multiple heterostructures. In this section we look at II-IV-V_2 CP compounds and assess their particular usefulness and advantage when used in highly integrated optical diagnostic devices that are applicable to environmental sensors, biological diagnostic tools, and medical diagnostics devices.

Figure 6 summarizes the lattice constants and band gap energies of several II-IV-phosphide and II-IV-arsenide and II-IV-nitride compounds, together with the lattice constants and band gap energies of group IV, III-V, and II-VI compound semiconductors that can act as potential substrates as well as for the formation of electrical and optical confinements for II-IV-V_2 nanocomposites and heterostructures.

Combining the requirements for optical confined birefringent CP compounds[8] with those compounds having the potential of room temperature (RT) ferromagnetism[24] considerably reduces the number of available material systems as shown in Table 1. Group III-nitride compounds GaN and InN are the primary candidates for the spintronic assisted SSMS device

structure, especially due to their strong potential to act not only as a ferromagnetic host but also due to their ability to act as templates for confined II-V-N_2 nanocomposites and heterostructures. Group III-arsenide and group III- phosphide do not show RT ferromagnetism, however they can act as mature substrate materials and confinement layers for embedded ferromagnetic II-V-P_2 and II-V-As_2 CP structures.

A comprehensive theoretical evaluation of potential ferromagnetic CP materials for spintronics was done by Erwin et al.,[24] who used a density-functional formalism to analyze 64 possible combination in the II-IV-V_2 materials class. This evaluation also considered the availability of closely lattice-matched semiconductor substrates. For the formation of 3d transition element doped nanocomposites and heterostructures the evaluation also has to take in account the availability of optically confined layers as discussed previous.[8]

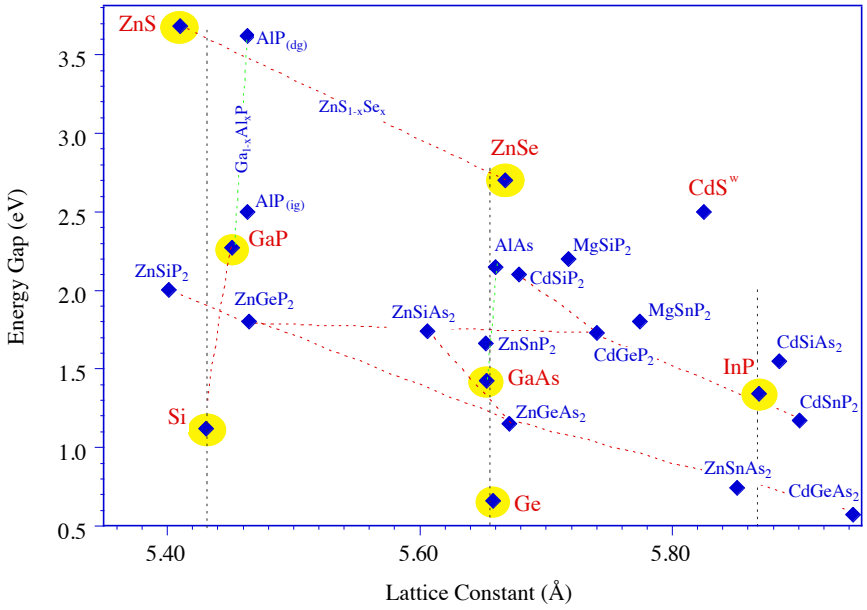

Fig. 6.
a) Energy gaps and lattice constants for the selected II-IV-P_2 and II-IV-As_2 compounds in relation to group IV, III-V and II-VI semiconductors (dg: direct gap, ig: indirect gap, p-dg: pseudo-direct gap).

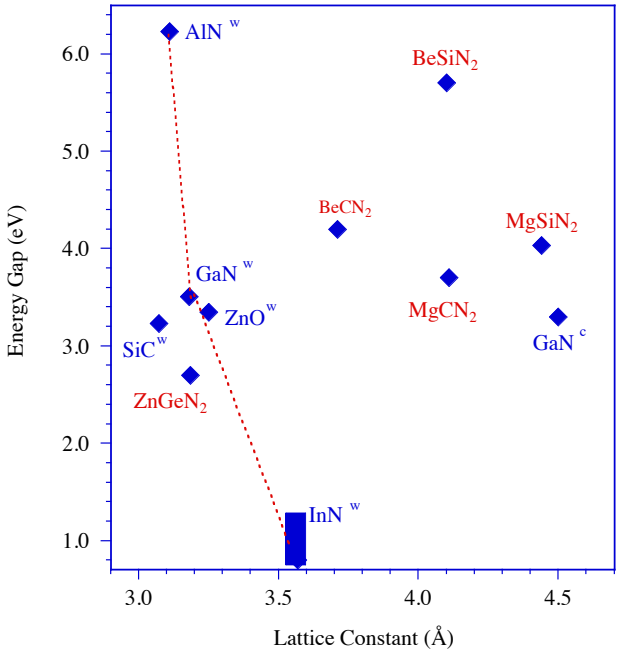

b) Energy gaps and lattice constants for the selected II-IV-N_2 compounds.

Table 1. Potential multifunctional CP material combinations

	3d-transition element doped semiconductors	Lattice-matched substrates	Confinement layers
Potential of having RT ferromagnetism	GaN	Sapphire, ZnO, AlN	$Ga_{1-x}Al_xN$
	InN	Sapphire, ZnO, AlN	$Ga_{1-x}In_xN$
Birefringent II-V-N_2 with potential of having RT ferromagnetism	$Zn(Ge_{1-x}Si_x)N_2$	wurtzite GaN, SiC, Sapphire	$Ga_{1-x}Al_xN$,
	(Mg or Be)SiN_2	zincblende $Ga_{1-x}Al_xN$	??
Birefringent II-V-P_2 with potential of having RT ferromagnetism	$Zn(Ge_{1-x}Si_x)P_2$	GaP and Si	$Ga_{1-x}Al_xP$
	$(Cd_{1-x}Zn_x)$ Ge P_2	GaAs, ZnSe	$Ga_{1-x}Al_xAs$
	$ZnSnP_2$	GaAs, ZnSe	$Ga_{1-x}Al_xAs$
	$Cd(Ge_{1-x}Sn_x)P_2$	InP	CdS
Birefringent II-V-As_2 with potential of having RT ferromagnetism	$Zn(Ge_{1-x}Si_x)As_2$	GaAs, ZnSe	$Ga_{1-x}Al_xAs$

3.3 THE GROWTH OF CONFINED GROUP II-IV-V_2 CP HETEROSTRUCTURES

The growth of group III-V semiconductor device structures has been proven most efficient by metal-organic chemical vapor deposition (MOCVD). It has been successfully applied to the growth of $(Ga_{1-x}Al_y)As$, $(Ga_{1-x}In_y)P$ and $(Ga_{1-y}Al_y)N$ device structures. Only the growth of indium rich $(In_{1-x}Ga_x)N$ alloys becomes a major challenge due to stoichiometric instabilities and low dissociation temperatures.[25] As successfully demonstrated for the CP compound $ZnGeP_2$, [26,27] growth by MOCVD should be possible for most of the II-IV-V_2 alloys, utilizing main-stream growth technology. SSMS devices operating on the near- and mid-infrared regime favor the exploration of optical confined $Zn(Ge_{1-y}Si_y)P_2$ heterostructures as well as the exploration of 3d-transition element doped $Zn(Ge_{1-y}Si_y)P_2$ QDs and nanocomposites.

Since room-temperature ferromagnetism has been already demonstrated for Mn doped GaMnN epilayers[28,29] the coupling of confined birefringent $Zn(Ge_{1-x}Si_x)N_2$ with ferromagnetic group III-nitride appears to be very promising for the design and fabrication of unique electro-/magneto-optical device structures. The fabrication and study of such systems will be crucial for the validation and understanding of electromagnetic wave propagation in ferromagnetic, birefringent waveguides.

The formation of miniaturized, integrated nonlinear device structures utilizing 1-dim birefringent photonic bandgap (PBG) structures is essential not only to enhance the nonlinearity, but also to minimize problems associated with walk-off and NLO device dimension. Such PBG structures can be formed in different configurations, two of them are illustrated in Fig. 7. Figure 7a shows a free-standing CP based PBG structures. Such structures can be fabricated either by focused ion beam (FIB) etching or a combination of nano-lithography and selective electro-chemical etching.

The width and spacing of such 1-dim PBG structures can be designed for optimized second harmonic generation (SHG) or for optical parameter oscillation (OPO) generation. In addition, such structures are also of interest for optically controllable electro-optic switches, nonlinear couplers, and optical gates in the visible and infrared (IR) wavelength regime as well as for coherent infrared laser light generation.

The second approach, shown in Figure 7b, employs as an example multiple $ZnGeP_2/GaP/ZnGeP_2$ heterostructures, which is a nearly lattice matched materials combination.

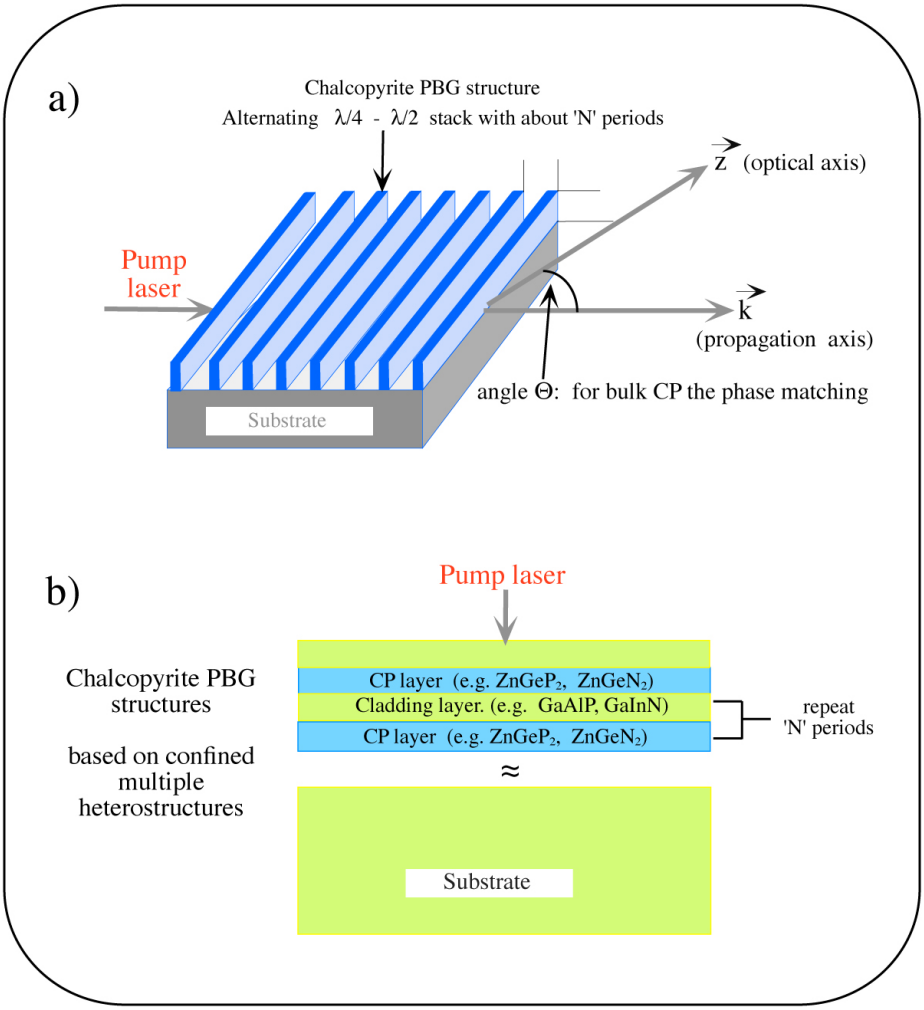

Fig. 7. Formation of PBG enhanced confined birefringent CP structures: a) in-plane structure, which can be formed in bulk CP and thick CP layers, and b) perpendicular 1-dim structures formed through multiple heterostructures.

The feasibility of constructing high grade $GaP/Zn(Si_xGe_{1-x})P_2$ and $Si/ZnGeP_2$ single hetero-structures and $GaP/ZnGeP_2/GaP$ multiple heterostructures has been successfully demonstrated by Xing et al.[26,27]. The transmission electron micrograph (TEM) shown in Fig. 8 demonstrates that abrupt interfaces between high purity epilayers can be achieved. One-dimensional PBG structures based on $ZnGeP_2/GaP$ multiple heterostructures can be also used as in-plane nonlinear optical elements, since $GaP/Ga_{1-x}Al_xP$ heterostructures provide a tunable optical confinement for the $ZnGeP_2$-$ZnSiP_2$ alloy system. NLO interactions in such confined birefringent layers provide an added degree of freedom consisting of the guide thickness, which can be used to achieve phase matching conditions and high gain under conditions where it is difficult or not possible in

bulk material.
Because the desired operational range is in the IR, $ZnGeP_2$ based PBG crystals will require refractive index modulations on a micrometer scale, which is easily achievable by conventional photo-lithography and heteroepitaxial growth methods.

The motivation for investigating $ZnGeP_2$ PBG crystals is their utility for comparative studies of the performance of novel PBG structures to conventionally phase matched bulk devices.

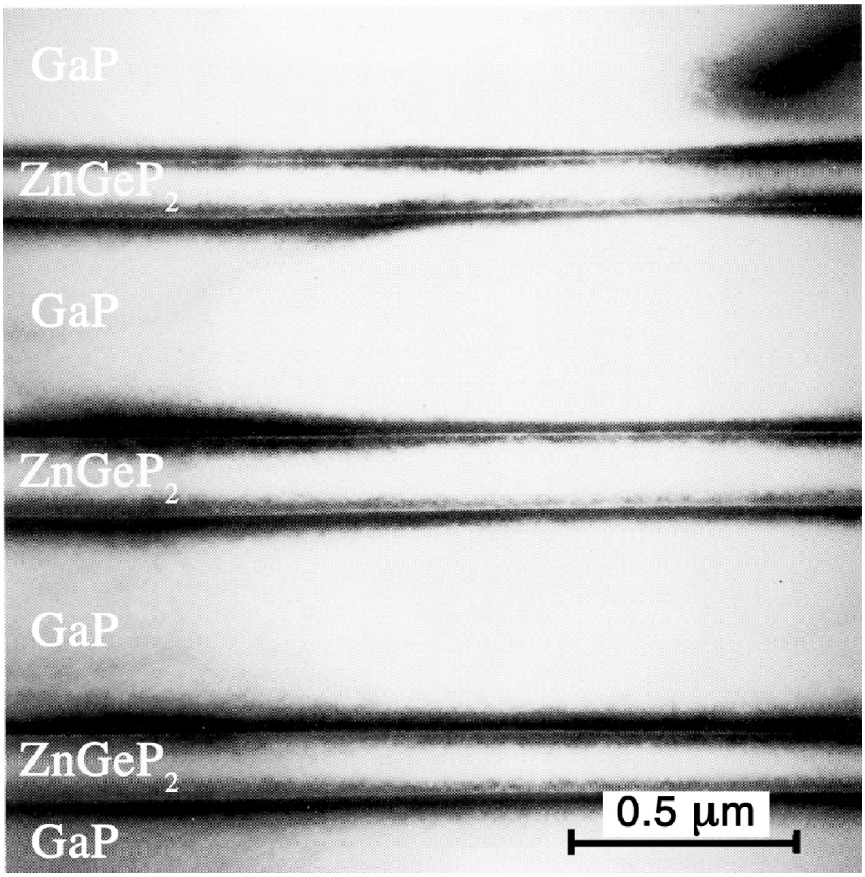

Fig. 8.
TEM cross-section of bright field image of a multiple GaP / $ZnGeP_2$ heterostructure grown on a GaP(001) substrate.[27]

For heteroepitaxial CP compound structures the critical issues to be addressed are:

a) evaluation and comparison of the defect chemistry of bulk materials with that of materials grown at lower temperatures by MOCVD and liquid phase epitaxy (LPE)
b) improvement of bulk materials, for instance homoepitaxial overgrowth of CP surfaces and heteroepitaxy of layers for antireflection coatings, etc.
c) device structures, for instance, p-n/n-p diode structures for detectors, and guided layers as active NLO elements for frequency-agile light generation

3.4 INTEGRATION OF PHOTONIC BANDGAP (PBG) STRUCTURES FOR DIFFRACTION AND WAVELENGTH FILTERS

PBG structures[15] are based on microstructured materials in which the dielectric functions ε between two materials is periodically modulated on a length scale comparable to the desired wavelength of light. Multiple interference between wave structures scattered from each unit cell

of the structure may open a "photonic bandgap" a range of frequencies within which no propagating electromagnetic field exists. Another key feature of PBG structures is their anomalous dispersion due to the periodic variation of permittivity with space. The development of optimized PBG structures for wavelength separation is a major research task requiring the study and optimization of the super-prism effect in PBG materials[30-33] with the existence of nonlinearity and birefringence present in CP material systems. By modifying the geometry of the PBG structures at the interface with the waveguides used in the proposed sensor structure, optimum coupling can be achieved. Fig. 9a shows examples of PBG structures formed in CP materials using conventional deposition and etching techniques. A concrete application would be an integrated optical diffraction element for spectral data analysis as depicted in Fig. 9b.

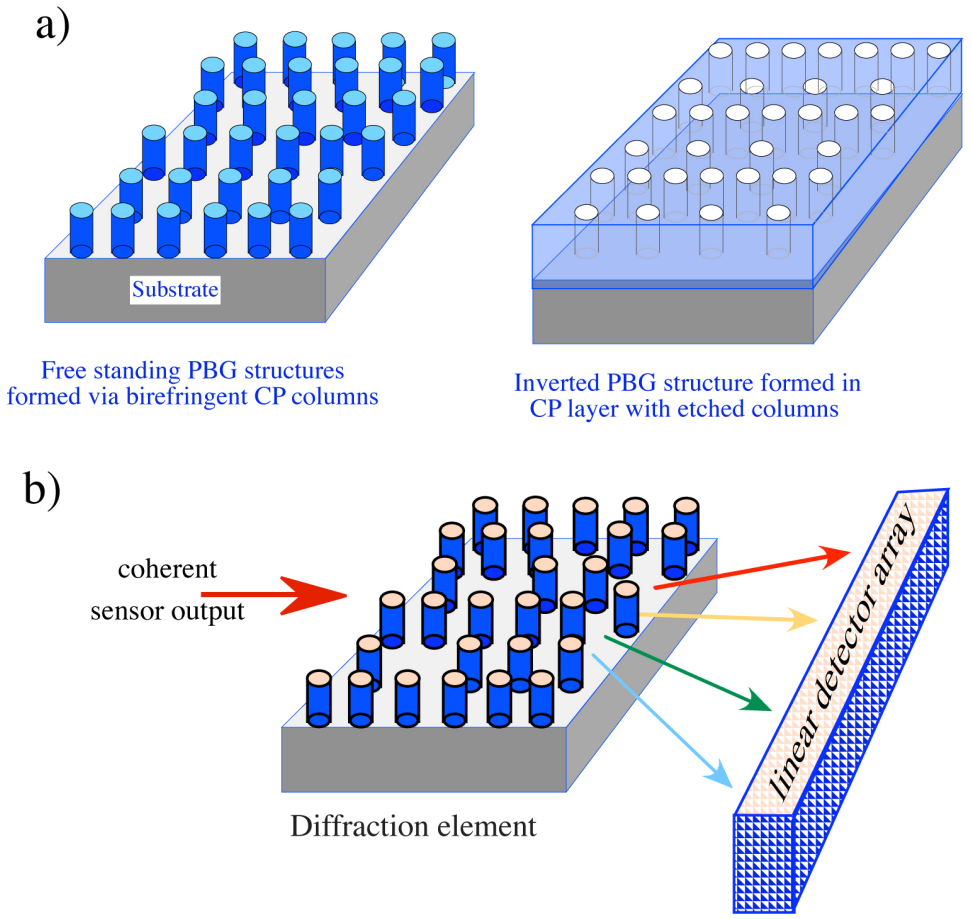

Fig. 9.
a) Nonlinear diffraction elements based on photonic bandgap structures fabricated in confined, birefringent CP layers**.**

b) Detection unit based on an integrated nonlinear CP based diffraction element and an array detector structure.

4. THEORETICAL FOUNDATIONS

In this section we review the theoretical foundations that support the concept, development and operation of SSMS structures. Our discussion is divided into three subsections: nonlinear waveguides, coupling to collector surface, and signal processing.

We begin by first displaying a flow chart in Fig. 10 that illustrates our overall integrated methodology for data acquisition and signal analysis. The circles within the flow chart indicate a logic decision path.

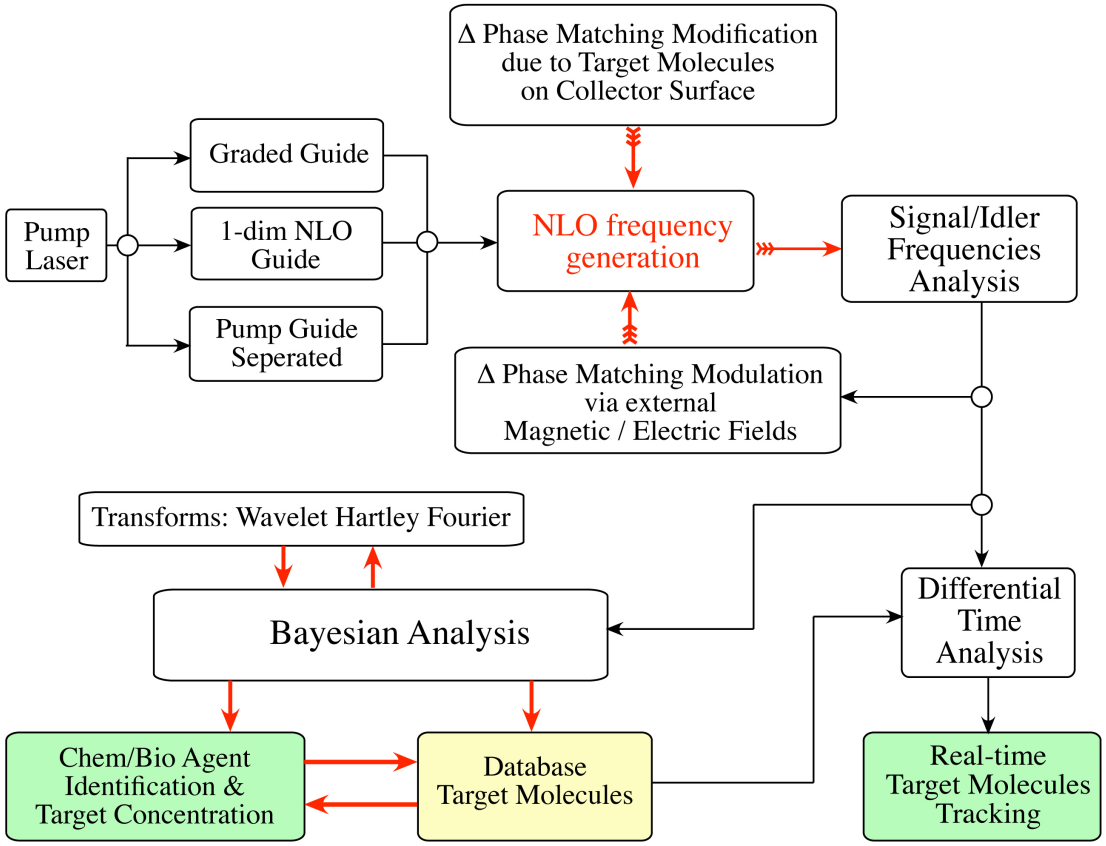

Fig. 10. Flow chart illustrating a typical logic path for target molecule identification, determination of target molecule concentrations, and real-time target molecule tracking.

4.1 NONLINEAR WAVEGUIDES

Chalcopyrite compound semiconductors are being used to achieve wavelength agility through much of the infrared spectrum. However, many applications, such as OPO and SHG, are limited by the phase-matching requirements of the bulk material. For example, $ZnGeP_2$, which is a potential CP material for the active layer in an SSMS structure, would make an excellent frequency doubler of 10.6 mm radiation (yielding 5.3μm radiation) but the phase matching conditions are difficult to achieve, which in turn places severe limitations on its conversion efficiency. The extraordinary wave index of refraction of $ZnGeP_2$ at 10.6μm is almost exactly equal to the ordinary wave index of refraction at 5.3μm making phase matching in bulk material marginal at best. This limitation, and corresponding limitations for other nonlinear processes, can be avoided by incorporating the $ZnGeP_2$, or other appropriate CP materials, in a waveguide structure. For example, the phase matching region for SHG can be considerably extended by coupling the pump into the guide in the fundamental, m = 0, mode and phase matching to the m = 2 mode of the second harmonic. We analyzed the phase matching conditions for SHG and OPO in birefringence birefringent nonlinear semiconductor waveguides and apply their results to the model system of $ZnGeP_2$ on a GaP substrate demonstrating the feasibility and efficient use of CP heterostructures. [34].

In order to achieve phase-matched conditions we considered that the optical axis of the $ZnGeP_2$

lies in the plane of the guide. In that case the angle between the direction of propagation of the wave in the guide and the optical axis of the guide material can be adjusted to achieve the phase matching condition. As shown below, we found that this can be accomplished for both SHG and OPO in $ZnGeP_2$ guides on GaP. Moreover, the waveguide geometry affords an additional opportunity for phase matching not available in bulk material. It is possible to couple radiation between different modes of the guide. We found that this will greatly extend the wavelength region over which phase-matched SHG can be achieved in a planar waveguide of $ZnGeP_2$.

We chose to examine the specific examples of OPO and SHG Type I phase matching in a $ZnGeP_2$ planar waveguide deposited on a GaP substrate and with GaP cladding, which represents the simplest confined CP structure possible. The optical, or z-axis, of the $ZnGeP_2$ lies in the plane of the guide as does the x- (or y-) axis for the optimum Type 1 non-linear coupling. For SHG Type I phase matching they considered that the guide is pumped in the TE mode with propagation at an angle Θ with respect to the optical axis of the $ZnGeP_2$.

Our results are shown in Figure 11. The corresponding phase matching angles for bulk $ZnGeP_2$ are shown for comparison. These results show phase matching angles quite similar to those of bulk $ZnGeP_2$[35] as would be expected for a guide this thick. This simply shows that phased matched SHG and OPO should be readily obtainable in waveguides of $ZnGeP_2$ operating in the m = 0 mode. The applicability of the bulk indices for the waveguide will depend on the guide thickness, growth method, doping level, lattice mismatch and internal strain. Bulk indices should be a good approximation for a well constructed 16 μm thick guide with reasonable lattice match as could be obtained with $ZnGeP_2$ on GaP.

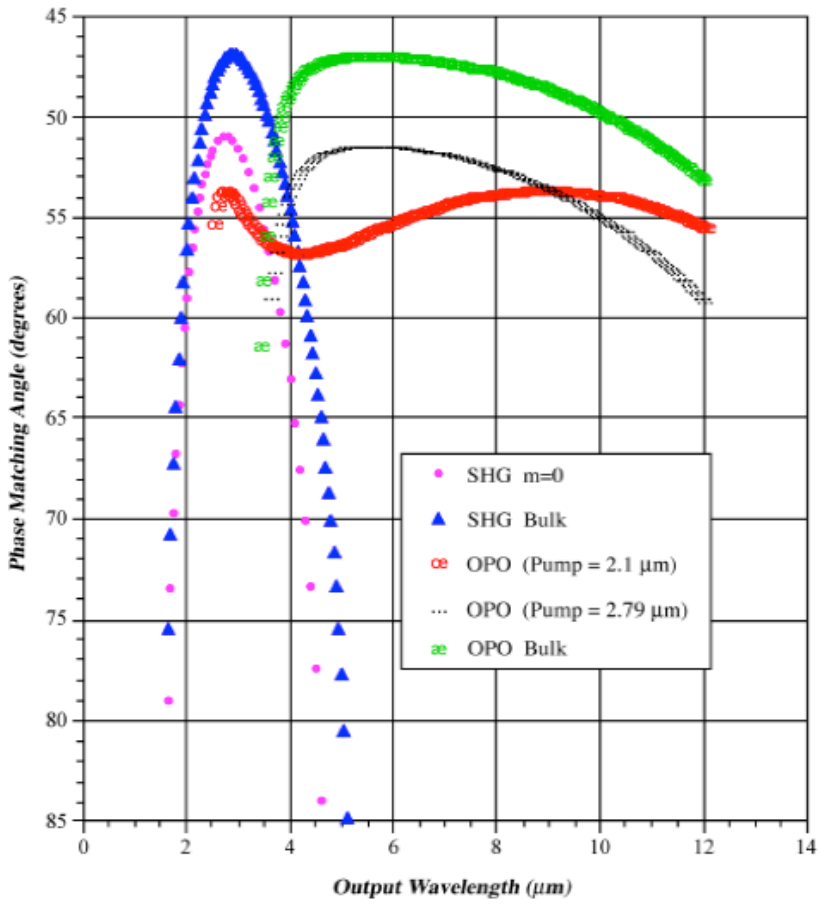

Fig. 11.
Calculated phase matching angles for SHG and OPO in a 16 μm $ZnGeP_2$ waveguide with a GaP substrate and cladding layer compared with similar curves for bulk material.

In Figure 12 we examined the case where coupling into the guide occurs in one mode of the guide, the nonlinear process within the guide couples energy to another mode and coupling out of the guide occurs from the second mode. Even though these calculations did not provide a detailed assessment of the strength of coupling, we estimated that nonlinear coupling from the m = 0 to the m = 2 mode, could be as large as 20% of the coupling to the m = 0 mode of the guide for similar phase matching conditions. For the purpose of illustration, we considered the case of SHG where the input wave is in the m = 0 mode with the second harmonic output considered in the m = 2 mode. Note that in this case phase matching for SHG can be obtained over wider wavelength region than for m = 0 to m = 0, or for bulk $ZnGeP_2$.

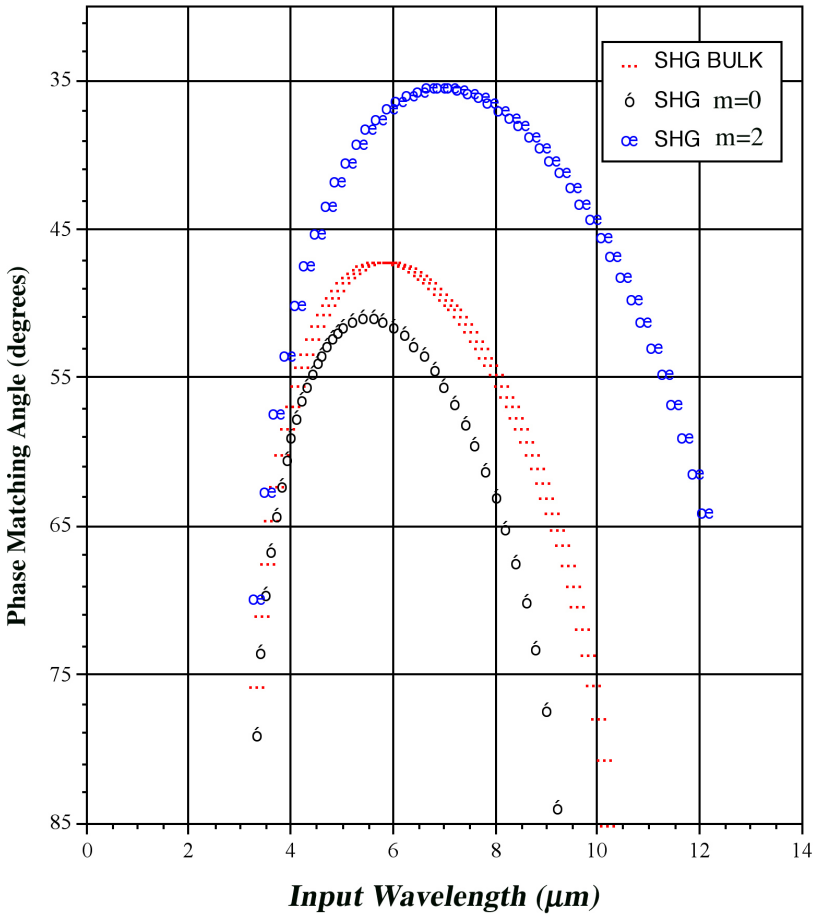

Fig. 12.
Calculated phase matching angles for SHG in the 16 μm $ZnGeP_2$ waveguide of Fig. 4 pumped in the m = 0 mode with output in the m = 2 mode compared to the m = 0 to m = 0 coupling of Fig. 13 and that of the bulk material.

4.2 COUPLING TO COLLECTOR SURFACE

Regardless of the probe configuration, a single channel waveguide where the probe, idler and signal waves propagate (Fig. 3), or a multiple channel guide where the probe, idler and signal waves propagate in separate channels (Fig. 4), it is essential to understand the probe's interaction with the collector surface when occupied by a concentration of target molecules in order to optimize the design parameters of the SSMS device structures. Clearly, a first principles modeling of this interaction, especially if multiple molecular species are present on the collector surface, is a challenging task. Nevertheless, it is imperative to have some understanding of physics involved in order to reduce costly experimentation and time. Our approach to this

problem will be incremental and complementary to experimental results. This will assure a validation of the modeling in a progressively stepwise fashion. A qualitative description of the detection system(s) was given in the Introduction. The following discussion is based on that description.

In the first step, the modeling of the SSMS device response has to focus on the interaction of the probe wave with the collector surface and its optical modification due to the presence of target molecules residing on the collector surface. Initially, as a first order approximation, a uniform distribution of a single molecular species on an infinite, homogenous collective surface will be assumed. The probe wave is taken as a single frequency propagating in a single channel guide. Effectively, this is a mean field approximation in which we limit our initial consideration to heavy and moderately heavy concentrations of target molecules. In this limit phase shifts due to the scattering by multiple target centers are coherent. Of course, the definition of heavy to moderately heavy concentrations also assumes a wavelength large compared to the inter-particle separation distance. Since little is known, either theoretically or experimentally, of how strong and in which frequency regime the presence of the molecules will affect the local dielectric function, a parametric approach will the used. In this approach, we assume different values of the dielectric coefficient and target concentrations in a parametric study in order to get a handle on the trend of the interactions: induced phase shifts and changes in absorption and the resulting frequency shift in the OPO process. Since the frequency shift in the OPO process is nonlinearly coupled to the phase and absorption shifts an iterative nonlinear fitting process is required to match the resulting frequency shift in the OPO process to the experimental data.

Once the model is developed for collector surface interaction, we move on to extend the model to include the generation and characteristics of the signal wave. In the OPO version of the detection unit the nonlinear generation of the signal and idler waves are functions of phases matching and the geometry of the resonance cavity. The phase matching in turn is dependent on the orientation of the optical axis of the material with respect direction of propagation of the probe wave. These are the elements to be added to the model. We will initially assume a lossless medium, but this may have to be modified depending on experimental results.

Slightly more complicated to model is the multiple channel version of the unit. In addition to fulfilling the phase matching conditions, we now have the added element of coupling between guides for which their geometries may not be symmetric. A measure of the strength of the interaction between the guides (the overlap integrals) is reflected in the "coupling coefficients." These coefficients, along with the structure of the signal wave will be calculated in a parametric study as a function of frequency, optic axis orientation and parallel waveguide geometries.

Finally, as was shown in section 4.1, it is possible to couple between other than the m = 0 modes of the guide. This possibility will be built into both versions of the detection unit.

4.3 SIGNAL PROCESSING

Real systems and real materials often do not approximate the ideal conditions assumed in model developments. The detection and discrimination of a particular molecular species and the determination of its concentration will be critically dependent on the data acquisition and the signal processing methodology. A general approach to the signal processing has been

developed. This approach is based on a conditional probabilistic reduction method known as Bayesian inference[36,37]. The uniqueness of employing the Bayesian inference lies in the fact that very precise physical models can be built directly into the method. For example, atomic form factors, which characterize the electronic structure of various target molecules, can be used for cellular image enhancement. Or, "structure factors" (analogues to those used in x-ray diffraction), which characterize the signature of various concentrations of target molecules. Models can also be constructed, which assess the influence of material defects (native point defects, surface decomposition, etc.), non-ideal interface sharpness, and composition and thickness variations, which may skew the signal information. The physical models can be determined from first principles or empirically from the system at hand. It may also be determined by a complementary pairing of theoretical and/or empirical, and/or stochastic methods, which includes the results of other signal processing methods. In a very real sense this methodology has the capacity to learn.

Bayesian inference has been known for over two hundreds, but has only recently been recognized and put into use in solving myriad of problems from pattern recognition to medical diagnostics. While it is a general technique applicable to many applications it is particularly suited to the problem of discrimination and concentration of multiple molecular species residing on the collector surface of an SSMS structure.

As a starting point, it is assumed that measurements result in a set of data that is represented by a column vector **D** of dimension 1 x N. If the data is multi-dimensional it is assumed that the pixels, or voxels, can be ordered in such a way as to produce the data vector **D**, i.e., $\mathbf{D}(\mathbf{d}_1,\mathbf{d}_2,\ldots,\mathbf{d}_N)$. The data **D** can be modeled by a vector function, **f,** and **n** a noise component:

$$\mathbf{D} = \mathbf{f}(\alpha) + \mathbf{n}, \tag{1}$$

α includes all the physical information, parameters, which arise in constructing a model to represent the data. The system's noise is represented by **n**, which in general is assumed to be additive, and as with the physical model function, the noise can be represented empirically, theoretically (Gaussian, for example, but need not be), or as a combination of both.

Because of the presence of noise, the inversion of Eq.(1) is non-unique and statistical procedures are necessary to obtain information about α. To accomplish this we employ Bayes' Theorem[37]:

$$P(\alpha \mid \mathbf{DI}) = [P(\mathbf{D} \mid \alpha\, \mathbf{I})\, P(\alpha \mid \mathbf{I})] / P(\mathbf{D} \mid \mathbf{I}), \tag{2}$$

where

$P(\alpha \mid \mathbf{DI})$ = **Posterior Probability** - Probability of finding (α | conditioned on | **DI**), where **I** stands for all other prior information. (3.a)

$P(\mathbf{D} \mid \alpha\, \mathbf{I})$ = **Likelihood Function** - Probability the measured data is observed if α, the hypothesis, is true. (3.b)

$P(\alpha \mid \mathbf{I})$ = **Prior Probability** - State of knowledge about the truth of α before analyzing current data. (For example, knowledge of experimental results

of various other measurements and/or other processing schemes.) (3.c)

$P(\mathbf{D} \mid \mathbf{I})$ = **Evidence** - Likelihood of observing the data, averaged over ALL possible values of solution parameters. (3.c)

For the case of Gaussian white noise the Likelihood Function may be written as,

$$P(\mathbf{D} \mid \boldsymbol{\alpha}\ \mathbf{I}) = \eta \exp(-[\mathbf{D} - \mathbf{f}(\boldsymbol{\alpha})]^{\dagger} \boldsymbol{\Sigma}^{-2} [\mathbf{D} - \mathbf{f}(\boldsymbol{\alpha})]), \quad (4)$$

where η is a normalization constant and $\boldsymbol{\Sigma}$ is the error covariant matrix for $\boldsymbol{\alpha}$. Model functions for $\mathbf{f}(\boldsymbol{\alpha})$ may be empirical, stochastic, theoretical, or a combination of any/all.

Two methods that have proven fairly successful and that are widely used in the estimation of $\boldsymbol{\alpha}$ are the *Maximum Likelihood* (ML) method [37,38] and the *Maximum A Posteriori* (MAP) method.[38] Both approaches are special cases of the Bayesian inference method.

Maximum Likelihood (ML) Method

This method corresponds to the case when no prior information is available for the estimation of $\boldsymbol{\alpha}$. Then, the parameter vector $\boldsymbol{\alpha}$ is estimated using

$$\nabla_{\alpha} P(\mathbf{D} \mid \boldsymbol{\alpha}\ \mathbf{I}) = 0. \quad (5)$$

For Gaussian noise this becomes

$$\nabla_{\alpha} [\mathbf{D} - \mathbf{f}(\boldsymbol{\alpha})]^{\dagger} \boldsymbol{\Sigma}^{-2} [\mathbf{D} - \mathbf{f}(\boldsymbol{\alpha})] = 0. \quad (6)$$

That is, Eq. (6) corresponds to the minimization of the nonlinear least-squares error. Thus one can use standard least-squares optimization procedures to estimate $\boldsymbol{\alpha}$.

Maximum A Posteriori (MAP) Method

In this method it is assumed that a prior estimate for $\boldsymbol{\alpha}$, $\boldsymbol{\alpha}_o$, is available and that the prior probability density is of Gaussian form.

For the special case when both the likelihood and the prior estimate are Gaussian, $\boldsymbol{\alpha}$ can be estimated from the following set of equations:

$$P(\boldsymbol{\alpha} \mid \mathbf{DI}) = N \exp[-(\boldsymbol{\alpha} - \boldsymbol{\alpha}_o)^{\dagger} \boldsymbol{\sigma}_{\alpha}^{-2} (\boldsymbol{\alpha} - \boldsymbol{\alpha}_o)], \quad (7)$$

and

$$\chi = [\mathbf{D} - \mathbf{f}(\boldsymbol{\alpha})]^{\dagger} \boldsymbol{\Sigma}^{-2} [\mathbf{D} - \mathbf{f}(\boldsymbol{\alpha})] + (\boldsymbol{\alpha} - \boldsymbol{\alpha}_o)^{\dagger} \boldsymbol{\sigma}_{\alpha}^{-2} (\boldsymbol{\alpha} - \boldsymbol{\alpha}_o) \quad (8)$$

$$\nabla_{\alpha} \chi = 0, \quad (9)$$

where N is a normalization constant and $\boldsymbol{\sigma}_{\underline{\alpha}} = \delta_{ij} \boldsymbol{\Sigma}$, i.e., only the diagonal elements of $\boldsymbol{\Sigma}$.

When the noise is taken as Gaussian the MAP method is equivalent to the minimization of χ. Equation (9) results in an estimate of $\boldsymbol{\alpha}$ clustered about $\boldsymbol{\alpha}_o$. The clustering, or difference, will depend on just how close to the true value(s) $\boldsymbol{\alpha}_o$ was to begin with. (For the special case of Gaussian noise the MAP method turns out to be equivalent to *Ridge Regression*.[39]

Moments of the Probability Distribution

Alternatively, an estimate of $\boldsymbol{\alpha}$ can be obtained by calculating its first moment:

$$\langle \boldsymbol{\alpha} \rangle = \int \boldsymbol{\alpha}\ P(\boldsymbol{\alpha}\ |\mathbf{DI})\ d\boldsymbol{\alpha}\ . \tag{11}$$

The second moment,

$$\langle \boldsymbol{\alpha}\boldsymbol{\alpha} \rangle = \int \boldsymbol{\alpha}\boldsymbol{\alpha}\ P(\boldsymbol{\alpha}\ |\mathbf{DI})\ d\boldsymbol{\alpha}\ , \tag{12}$$

gives the variance(s) on the estimate of $\boldsymbol{\alpha}$.

Physical Model Function

The physical model function **f** containing a set of parameters, such as the concentration of the target molecules, frequencies, decay rates, chirp rates (or any other quantities, which may be encountered in the measurement process) can be expanded in a set of basis functions $\mathbf{G}_j$:

$$\mathbf{f}(\boldsymbol{\alpha}) = \sum B_j\ \mathbf{G}_j(\boldsymbol{\alpha}), \tag{13}$$

where the B_j are the associated expansion coefficients. Appropriately constructed wavelets[39-41] obtain directly from the measured data on known samples is an example of the basis functions that may be employed.

5. SUMMARY

In this Chapter, we provided an introduction on the use of multifunctional, confined group II-IV-V_2 chalcopyrite materials for compact, highly-sensitive Solid State Molecular Sensor (SSMS) devices. The SSMS is a unique patented concept, which is based on nonlinear processes that enable the detection, discrimination and real-time tracking of specified chemical and biological agents. It does so by employing a highly nonlinear detection scheme, where phase and amplitude information over a large spectral range are translated into a characteristic frequency spectra, which can then be analyzed with a high degree of accuracy.

Through a critical review and assessment of the physical and optical properties of chalcopyrite compounds, $Zn(Ge_{1-x}Si_x)P_2$ and $Zn(Ge_{1-x}Si_x)N_2$ are identified as the two most promising materials systems for multifunctional SSMS device structures. An important aspect in the identification of these two systems for confined CP device structures is their compatibility with their group III-V companions that will allow the integration with established thin-film materials technologies.

The fabrication of SSMS device structures by MOCVD has been shown for the model system GaP/$ZnGeP_2$/GaP, demonstrating the feasibility of growing high-quality multiple confined chalcopyrite layers. MOCVD is particularly suited for the growth of group II-IV-V_2 compounds due to the availability of high-quality organometallic precursors and nearly lattice matched III-V compounds, serving as substrates and confinement layers in multiple heterostructures.

Using the model system of $ZnGeP_2$/GaP our theoretical analysis of nonlinear propagation for the generation of coherent infrared laser light by second-harmonic generation and optical parametric oscillation showed that such a structure has the added flexibility that phased matched coupling can occur between various modes of the guide. Moreover, since the coupling is a function of the thickness of the guide an additional degree of freedom is realized. These added degrees of freedom will allow for high gain under conditions where it is difficult or impossible to achieve in

bulk material.

Critical to the detection and accurate discrimination of various target molecules attached to the collector surface is the signal process methodology. Our choice is Bayesian inference. This unique and powerful technique is not only compatible with our data acquisition scheme but, just as importantly, uses all prior and new information (empirical, theoretical, stochastic, or any combination of them) as acquired allowing for a continual updating of the targets' database. In this sense the Bayesian method has the capacity to learn.

While the primary focus in this chapter was on the detection and discrimination of chemical and/or biological molecular target species, the unique properties of SSMS device structures paves the way for a myriad of applications, which include but are not limited to: remote screening of air and water pollutants; monitoring of surface corrosion/etching processes; bio-medical testing and drug development.

6. REFERENCES

[1] "Chemical and Biochemical Sensing with Optical Fibers and Waveguides," ed. G. Boisdé and A. Harmer, ISBN 0-89006-737-6; Artech House, Inc, Norwood, MA 02062 (1996).

[2] P. A. Budni, K. Ezzo, P. G. Schunemann, S. Minnigh, J. C. McCarthy and T. M. Pollak, OSA Proceedings on Advanced Solid-State Lasers. Vol.10, Proceedings of the Topical Meeting , pp. 335-8 (1991).

[3] P. A. Budni, P. G. Schunemann, M. G. Knights, T. M. Pollak and E. P. Chicklis, OSA Proceedings on Advanced Solid-State Lasers. Vol.13. Proceedings of the Topical Meeting , pp. 380-3 (1992).

[4] Y. M. Andreev, P. P. Geiko, G. M. Krekov and O. A. Romanovskii, Proceedings of the SPIE - The International Society for Optical Engineering **1811**, pp. 367-70 (1992).

[5] K. Stoll, J.-J. Zondy and O. Acef, Optics Letters **22**, pp. 1302-1304 (1997).

[6] N. P. Barnes, K. E. Murray, M. G. Jani, P. G. Schunemann and T. M. Pollak, J. Opt. Soc. Am. B **15**(1) pp. 232-238 (1998).

[7] US Patent No. **6,442,319**, "Chalcopyrite Based Nonlinear Waveguided Heterostructure Devices and Operating Methods," N. Dietz and K.J. Bachmann, Aug. 27, 2002.

[8] N. Dietz and F.L. Madarasz, Mater. Sci. & Eng. B, Vol **97**(2) pp. 182-195 (2003).

[9] US Patent No. **6,834,149**, "Optically Confined Birefringent Chalcopyrite Heterostructure Devices and Operating Methods," N. Dietz, F. Madarasz, and D. Krivoshik, December 22, 2004.

[10] N. Dietz, F. Madarasz, and R. Inguva, Proc. SPIE Vol. **5912**, pp. 129-138 (2005).

[11] "Ternary Chalcopyrite Semiconductors: Growth, Electronic Properties, and Applications," ed. J. L. Shay and J. H. Wernick, Oxford, New York, Pergamon Press [1975].

[12] M. M. Tilleman and A, Englander, Optical Engineering **39**(3), pp. 758-762 (2000).

[13] S. N. Rashkeev, S. Limpijumnong and W. R. L. Lambrecht, Phys. Rev. B. **59**(2), pp. 2737 - 2748 (1999).

[14] K. L. Vodopyanov, F. Ganikhanov, J. P. Maffetone, I. Zwieback, and W. Ruderman, Optics Letters **25**(11) pp. 841-843 (2000).

[15] "Photonic crystals: molding the flow of light," ed. R. D. Meade, J. D. Joannopoulos, J. N.

Winn, Princeton University Press, ISBN: 0691037442, (1995).

[16] Yu-Jun Zhao, W. T. Geng, A. J. Freeman, T. Oguchi, Phys. Rev. B **63**, pp. 201202 (2001).

[17] G. A. Medvedkin, K. Hirose, T. Ishibashi, T. Nishi, V. G. Voevodin, and K. Sato, J. Crystal Growth, **236**(4) pp. 609-612 (2002).

[18] K. Sato, G. A. Medvedkin, T. Ishibashi, S. Mitani, K. Takanashi, Y. Ishida, D. D. Sarma, J. Okabayashi, A. Fujimori, T. Kamatani and H. Akai, J. Phys. Chem. Solids, **4**(9-10), pp. 1461-1468 (2003).

[19] V.V. Popov, G.A. Medvedkin, Solid State Communications, **132**(8) pp. 561-565 (2004).

[20] H. Yi and Hy. Park, Physica B **359-361** pp. 1466-1468 (2005).

[21] O. Madelung, "Semiconductor Physics; Basic Data of Semiconductors," 2nd ed., Springer Verlag, ISBN 3540608834 (1996).

[22] V.G. Dmitriev, G.G. Gurzadyan, and D.N. Nikogosyan, Handbook of Nonlinear Optical Crystals, 2nd ed., Springer Series in Optical Sciences. Eds.: A.L. Schawlow, K. Shimoda, A.E. Siegman, T. Tamir. Vol. 64; ISBN 3-540-61275-0 (1997).

[23] S.F. Marenkin, V.M. Novotortsev, K.K. Palkina, S.G. Mikhailov, V.T. Kalinnikov, Inorganic Materials **40**(2) pp.93 - 95 (2004).

[24] Steven C. Erwin, Igor Zuticacute, Nature Materials **3**(6) pp. 410-414 (2004).

[25] "Indium-nitride growth by HPCVD: Real-time and ex-situ characterization," N. Dietz, book chapter 6 in "III-Nitrides Semiconductor Materials", ed. Z.C. Feng, Imperial College Press, ISBN 1-86094-636-4, pp. 203-235 (2006).

[26] G.C. Xing, K.J. Bachmann, G.S. Solomon, J.B. Posthill and M.L. Timmons, J. Crystal Growth **94**(2) pp. 381-386 (1989).

[27] G.C. Xing and K.J. Bachmann, J. Crystal Growth **147**(1/2), pp. 35-8 (1995).

[28] M. Kane, A. Asghar, A.M. Payne, C.R. Vesta, M. Strassburg, J. Senawiratne, Z J. Zhang, N. Dietz, C. Summers, I.T. Ferguson, Semicond. Sci. Technol. **20** L5–L9 (2005).

[29] M.H. Kane, M. Strassburg, A. Asghar, Q. Song, S. Gupta, J. Senawiratne, C. Hums, U. Haboeck, A. Hoffmann, D. Azamat, W. Gehlhoff, N. Dietz, Z.J. Zhang, C.J. Summers, I.T. Ferguson, Proc. SPIE Vol. **5732** pp. 389-400 (2005).

[30] H. Kosaka, T. Kawashima, A. Tomita, M. Notomi, T. Tamamura, T. Sato, S. Kawakami, Phys. Rev. B **58**, p 10096 (1998).

[31] H. Kosaka, T. Kawashima, A. Tomita, M. Notomi, T. Tamamura, T. Sato, S. Kawakami, J. Lightwave Technology **17** p. 2032 (1999).

[32] B. Momeni and A. Adibi, Appl. Phys. B **77**, pp.555-560 (2003).

[33] B. Momeni, J. Huang, M. Soltani, M. Askari, S. Mohammadi, M. Rakhshandehroo, and A. Adibi, Opt. Express **14**, pp.2413-2422 (2006).

[34] J. O. Dimmock, F. L. Madarasz, N. Dietz and K. J. Bachmann, Applied Optics **40**(9), pp. 1438-1441 (2001).

[35] "Emergence of chalcopyrites as nonlinear optical materials," M. C. Ohmer and R. Pandey, (eds.), Materials Reseach Bulletin, Vol. **23**(7) (1998).

[36] G. L. Brethorst, ISBN: 038796871, Springer-Verlag, New York (November 1988).

[37] D. S. Sivia, "Data Analysis: A Bayesian Tutorial," ISBN: 0198517629, New York: Oxford University Press (1996).

[38] William K. Pratt, "Digital Processing," ISBN: 0471018880, John Wiley & Sons Inc., New York (1978).

[39] H.C. Andrews and B. R. Hunt, "Digital Image Restoration," Prentice-Hall, Englewood Cliffs, N.J. (1977).

[40] Gerald Kaiser, "A Friendly Guide to Wavelets," ISBN: 0817637117, Birkhäuser, Boston, (1994).

[41] Charles K. Chui, "An Introduction to Wavelets," ISBN: 0121745848, Academic Press, New York (1992).